

hep-ph/0607002

CERN-PH-TH/2006-110

UMN-TH-2509/06

FTPI-MINN-06/23

What if supersymmetry breaking appears below the GUT scale?

John Ellis¹, Keith A. Olive² and Pearl Sandick²

¹*TH Division, CERN, Geneva, Switzerland*

²*William I. Fine Theoretical Physics Institute,
University of Minnesota, Minneapolis, MN 55455, USA*

Abstract

We consider the possibility that the soft supersymmetry-breaking parameters $m_{1/2}$ and m_0 of the MSSM are universal at some scale M_{in} below the supersymmetric grand unification scale M_{GUT} , as might occur in scenarios where either the primordial supersymmetry-breaking mechanism or its communication to the observable sector involve a dynamical scale below M_{GUT} . We analyze the $(m_{1/2}, m_0)$ planes of such sub-GUT CMSSM models, noting the dependences of phenomenological, experimental and cosmological constraints on M_{in} . In particular, we find that the coannihilation, focus-point and rapid-annihilation funnel regions of the GUT-scale CMSSM approach and merge when $M_{in} \sim 10^{12}$ GeV. We discuss sparticle spectra and the possible sensitivity of LHC measurements to the value of M_{in} .

1 Introduction

The primary phenomenological reason for expecting supersymmetry to appear at the TeV scale is to ensure the naturalness of the hierarchy of mass scales in fundamental physics [1]. It is also known to facilitate the construction of simple Grand Unified Theories (GUTs) with no intermediate mass scale, if supersymmetry appears around the TeV scale [2]. These two motivations for low-energy supersymmetry arise specifically in theories with large GUT and Planck mass scales, and are supplemented by other motivations for low-energy supersymmetry, such as cold dark matter [3] and the existence of a light Higgs boson [4].

Supersymmetry is all very nice, but it must be broken, and there is no consensus how this occurs. Presumably the origin of supersymmetry breaking is with a gravitino mass in local supersymmetry [5], but the mechanism for gravitino mass generation is still unclear, as is the manner whereby this breaking is communicated to the supersymmetric partners of observable particles [6]. It is often supposed that supersymmetry is initially broken in some Polonyi or hidden sector of the theory [7,8], and is then transmitted to the spartners of Standard Model particles by either gravitational-strength interactions or some high-scale gauge interactions.

In phenomenological treatments of supersymmetry, the effective observable magnitudes of these supersymmetry-breaking parameters at low scales are then calculated using the renormalization-group equations (RGEs) of the effective low-energy theory, which is typically taken to be the minimal supersymmetric extension of the Standard Model (MSSM) [9]. One often assumes that the soft supersymmetry-breaking parameters are universal at some high input scale, and we term the resulting constrained model the CMSSM [10–14]. However, it should be stressed that not all models of supersymmetry breaking, e.g., in string theory yield such universal input parameters [15].

There is also the question of what input scale should be used to initialize the renormalization-group running of the soft supersymmetry-breaking parameters. In most CMSSM studies, this is taken to be the supersymmetric GUT scale $M_{GUT} \sim 2 \times 10^{16}$ GeV, but this assumption may be questioned. In general, it should probably be taken as approximately equal to the lowest among the dynamical scales in the Polonyi or hidden sector where supersymmetry is originally broken, and the scales of the interactions that transmit this breaking to the observable MSSM particles.

One could well imagine scenarios in which the input scale is *above* the GUT scale, e.g., if supersymmetry breaking and its mediation are characterized by the Planck or the string scale. In this case, the soft supersymmetry-breaking gaugino masses $m_{1/2}$ would evolve to-

gether down to the GUT scale, where they would still be universal, diverging at lower scales according to the conventional MSSM RGEs. On the other hand, the soft supersymmetry-breaking scalar masses m_0 would not in general be universal at the GUT scale M_{GUT} , but would be different for different GUT multiplets. For example, in conventional SU(5) the scalar masses of the spartners of the d_R and ℓ_L would be identical, but different from those of the spartners of the q_L, u_R and e_R , since they come from $\bar{5}$ and 10 representations, respectively. On the other hand, in flipped SU(5) the groupings would be u_R, ℓ_L and q_L, d_R , with the e_R different again, whereas only in SO(10) would all the soft supersymmetry-breaking scalar masses of the quarks and leptons be universal (but not those of the Higgs bosons). These would be interesting scenarios to study, but are not the objects of this paper.

Here we study instead the equally (if not more) plausible case in which universality applies to the parameters $m_{1/2}$ and m_0 at some input scale *below* the GUT scale. This might occur if the scale at which supersymmetry is broken dynamically in some hidden sector is smaller than the M_{GUT} , for example due to the v.e.v. of some condensate that appears at a lower scale. A partial analogue may be the chiral-symmetry breaking quark condensate in QCD, which generates a ‘soft’ effective quark mass that ‘dissolves’ at scales above Λ_{QCD} . Alternatively, perhaps ‘hard’ supersymmetry breaking in the hidden sector is communicated to the observable sector by loops of particles weighing less than M_{GUT} , which ‘dissolve’ at high scales. In any such sub-GUT CMSSM scenario, the gaugino masses would evolve in the same way as the gauge couplings at the leading (one-loop) level, but from a different starting point, so that their effective values at low energies would be less separated than they are in the usual GUT CMSSM scenario. Likewise, the effective values of the soft supersymmetry-breaking scalar masses at low energies would also be more similar in a sub-GUT CMSSM than in the usual scenario.

The renormalization of the gauge couplings would always be the same in sub-GUT CMSSM scenarios, and the successful coupling unification of supersymmetric GUTs would therefore be preserved. However, because the renormalizations of the soft supersymmetry-breaking parameters would differ in these scenarios, as we demonstrate and explain, the regions of the $(m_{1/2}, m_0)$ plane allowed by experiments and cosmology in such a sub-GUT CMSSM scenario may be very different from those allowed in the usual GUT CMSSM scenario. For example, the impact of the LEP constraint on the MSSM Higgs h is more marked, because the reduced dependence on $m_{1/2}$ of $m_{\tilde{t}}$ (which largely controls m_h) implies that only values of $m_{1/2}$ larger than those required in the GUT CMSSM are allowed in a sub-GUT CMSSM.

However, the most dramatic aspect of a sub-GUT CMSSM scenario may be the altered

form of the constraint imposed by the relic density of supersymmetric cold dark matter. We assume that R parity is conserved, so that the lightest supersymmetric particle (LSP) is stable, and hence should be present in the Universe today as a relic from the Big Bang. We further assume that the lightest supersymmetric particle (LSP) is the neutralino χ . In the usual GUT CMSSM scenario, one may distinguish three well-separated, generic regions of the $(m_{1/2}, m_0)$ plane that are allowed by the dark matter constraint imposed by WMAP [16] on the relic χ density: the coannihilation region [17], the focus-point region [18] and the rapid-annihilation funnel region [11, 19]. In sub-GUT CMSSM models, these regions tend to merge in a striking way as the input supersymmetry-breaking scale is reduced. This behaviour is understandable, stemming from the relations between different MSSM particle masses. In the coannihilation region, the neutralino and lighter stau have very similar masses, whereas in the focus-point region $|\mu| \sim m_W$, and in the funnel region $m_\chi \sim m_A/2$. Because of the different degrees of renormalization of the sparticle masses in sub-GUT CMSSM models, the relations between these masses and the underlying parameters $m_{1/2}$ and m_0 change, causing the three different regions to move and ultimately merge.

2 Experimental, phenomenological and cosmological constraints in the CMSSM

We begin by briefly discussing the constraints imposed on a standard GUT CMSSM model. This will serve as a baseline for comparison with the sub-GUT CMSSM models which are the focus of this paper. In Fig. 1(a), we show the $(m_{1/2}, m_0)$ plane in the GUT CMSSM model for $\tan\beta = 10$ and $m_t = 172.5$ GeV [20]. Among the relevant phenomenological constraints shown are the limits on the chargino mass: $m_{\chi^\pm} > 104$ GeV [21], shown as the near-vertical (black) dashed line at low $m_{1/2}$, and on the Higgs mass: $m_h > 114$ GeV [22], shown as the near-vertical (red) dot-dashed curve at $m_{1/2} \approx 400$ GeV¹. Another phenomenological constraint is the requirement that the branching ratio for $b \rightarrow s\gamma$ be consistent with the experimental measurements [24]. These measurements agree with the Standard Model, and therefore provide bounds on MSSM particles [25] and hence the $(m_{1/2}, m_0)$ parameter space. At $\tan\beta = 10$ and $\mu > 0$, the bound due to $b \rightarrow s\gamma$ is weak, as is shown by the green shaded region at low $m_{1/2}$ and m_0 . Typically, the $b \rightarrow s\gamma$ constraint is more important for $\mu < 0$, but it is also relevant for $\mu > 0$, particularly when $\tan\beta$ is large. Finally, we display with pink

¹Here and throughout this paper, we use `FeynHiggs` [23] for the calculation of m_h . We do not allow for the possible theoretical and parametric errors in the `FeynHiggs` results, which would allow values of $m_{1/2} \sim 80$ GeV smaller for the value of $\tan\beta = 10$ considered here.

shading the regions of the $(m_{1/2}, m_0)$ plane that are favoured by the BNL measurement [26] of $g_\mu - 2$ at the $2\text{-}\sigma$ level, as calculated in the Standard Model using e^+e^- data ².

As already mentioned, we assume that R parity is conserved, so that the LSP is stable, and we further assume that the LSP is the lightest neutralino χ . Also shown as the turquoise shaded regions in Fig. 1 are the parts of the $(m_{1/2}, m_0)$ plane where the relic density of the neutralino LSP χ falls within the range preferred by WMAP, namely $0.085 < \Omega_{CDM} < 0.119$ at the $2\text{-}\sigma$ level [16]. The cosmological region shown in panel a) corresponds to the $\chi - \tilde{\tau}$ co-annihilation strip [17]. The ‘bulk’ region which existed formerly at small $m_{1/2}$ and m_0 is excluded for $\tan\beta = 10$ with $m_t = 172.5$ GeV by the Higgs mass bound.

There is an additional region of acceptable relic density in the GUT CMSSM model, known as the focus-point region [18], which is found at rather higher values of m_0 . As m_0 is increased, the value of μ at the electroweak scale which is required in the GUT CMSSM to obey the electroweak symmetry breaking conditions eventually begins to drop. When $\mu \lesssim m_{1/2}$, the composition of the LSP gains a strong Higgsino component, and the relic density begins to drop precipitously. As m_0 is increased further, there is no longer any consistent solution for μ . The focus-point region is not seen in panel a), since it occurs at $m_0 > 1000$ GeV for the value $m_t = 172.5$ GeV assumed here. However, the focus-point region does appear in the sub-GUT CMSSM models discussed below.

Finally, another region of interest is that created by rapid annihilation via the direct-channel pole mediated by the Higgs pseudoscalar A when $m_\chi \sim \frac{1}{2}m_A$ [11,19]. We recall that the heavier neutral scalar Higgs boson H is almost degenerate with the pseudoscalar boson A , but plays a much less significant role in the annihilation process. Since the heavy scalar and pseudoscalar Higgs masses decrease as $\tan\beta$ increases, whilst m_χ is almost fixed by the value of $m_{1/2}$ and is largely independent of m_0 , eventually $2m_\chi \simeq m_A$ at any fixed value of $m_{1/2}$. The direct-channel annihilation then becomes rapid, yielding a ‘funnel’ of parameters with acceptable relic density, that extends to large $m_{1/2}$ and m_0 at large $\tan\beta$. This region is not present in the GUT CMSSM model at $\tan\beta = 10$, but we will see that it appears when the input scale for supersymmetry breaking is reduced. The funnel due to rapid annihilation via the light Higgs scalar is excluded in this case by the chargino mass bound, as well as by the Higgs mass bound.

²The $\pm 1 - \sigma$ range of the possible supersymmetric contribution to $g_\mu - 2$ is indicated by dashed lines. In view of the uncertainty surrounding the Standard Model contribution to $g_\mu - 2$, we consider the implementation of this constraint as purely indicative.

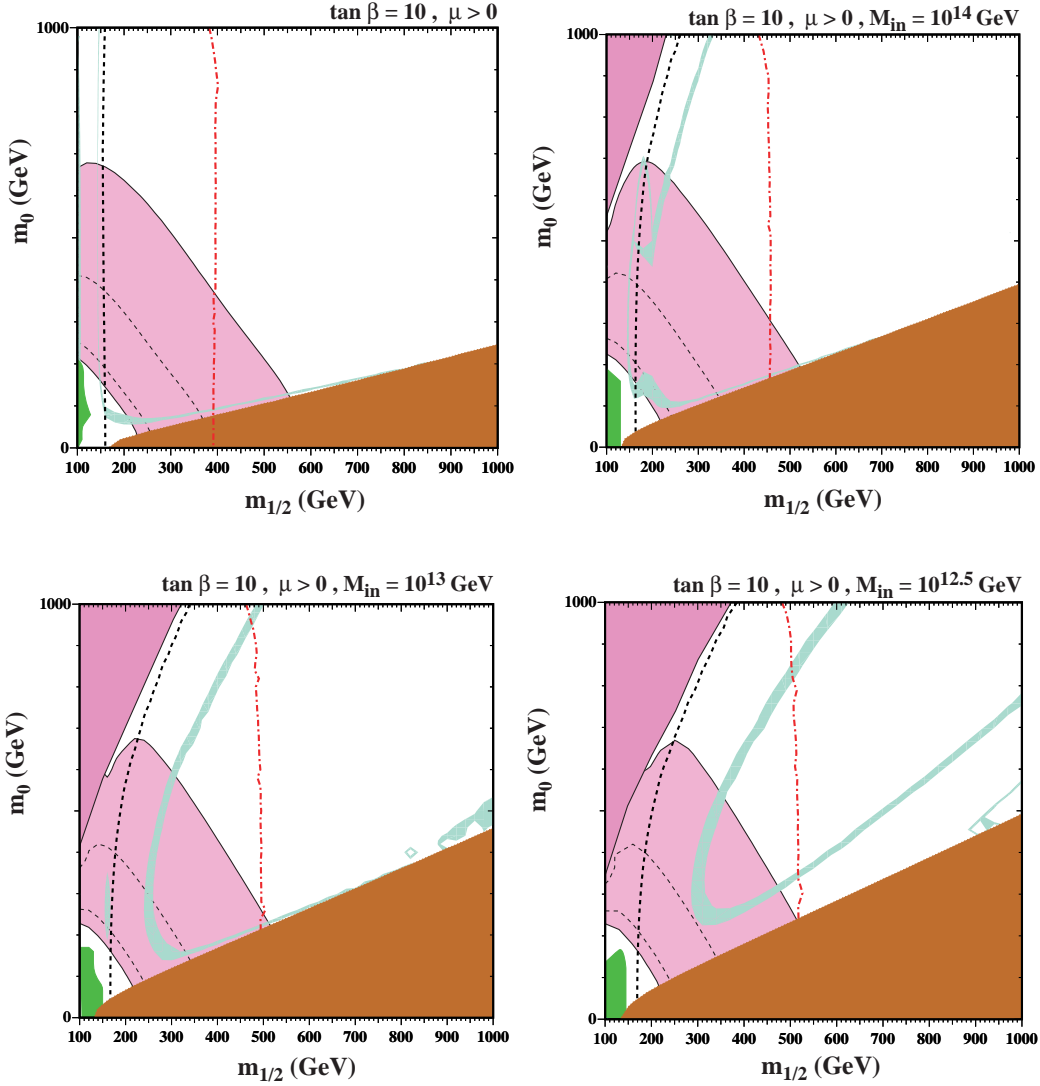


Figure 1: *Examples of $(m_{1/2}, m_0)$ planes with $\tan \beta = 10$ and $A_0 = 0$ but with different values of M_{in} . (a) The CMSSM case with $M_{in} = M_{GUT} \sim 2 \times 10^{16}$ GeV, (b) $M_{in} = 10^{14}$ GeV, (c) $M_{in} = 10^{13}$ GeV and (d) $M_{in} = 10^{12.5}$ GeV. In each panel, we show the regions excluded by the LEP lower limits on MSSM particles, those ruled out by $b \rightarrow s\gamma$ decay [24, 25] (medium green shading), and those excluded because the LSP would be charged (dark red shading). The region favoured by the WMAP range $\Omega_{CDM}h^2 = 0.1045^{+0.0072}_{-0.0095}$ has light turquoise shading. The region suggested by $g_\mu - 2$ is medium (pink) shaded.*

3 Lowering the universality scale for soft supersymmetry breaking

We now explore the consequences of reducing below M_{GUT} the scale at which universality is assumed for the supersymmetry-breaking parameters $m_{1/2}$ and m_0 , as might occur if the underlying supersymmetry-breaking mechanism and/or the mechanism for communicating it to the observable sector are characterized by a dynamical scale $M_{in} < M_{GUT}$. One could, in principle, imagine that the scales at which the $m_{1/2}$ and m_0 parameters are universal might be different, but we do not consider such a possibility here ³.

As already mentioned, at the one-loop level the renormalizations of the gaugino masses $M_a (a = 1, 2, 3)$ are identical with those of the corresponding gauge coupling strengths α_a , so that in a sub-GUT CMSSM

$$M_a(Q) = \frac{\alpha_a(Q)}{\alpha_a(M_{in})} M_a(M_{in}), \quad (1)$$

where the input gaugino masses $M_a(M_{in}) = m_{1/2}$ by assumption. By comparison, in the usual GUT CMSSM, the values of the gaugino masses would already be different at the lower scale M_{in} : $M_a(M_{in}) = (\alpha_a(M_{in})/\alpha(GUT)) \times m_{1/2}$. Therefore, in the sub-GUT CMSSM scenario, the low-energy effective soft supersymmetry-breaking gaugino masses differ from each other by smaller amounts than in the usual GUT CMSSM.

The soft supersymmetry-breaking scalar masses of the different squark and slepton flavours and Higgs bosons m_{0_i} are renormalized below the universality scale by both gauge interactions and Yukawa interactions. The latter are important for the stop squarks and the Higgs multiplet coupled to them, and for the sbottom squarks, stau sleptons and the other Higgs multiplet at large $\tan\beta$. The net effects of these renormalizations may be summarized as follows:

$$m_{0_i}^2(Q) = m_{0_i}^2(M_{in}) + C_i(Q, M_{in})m_{1/2}^2, \quad (2)$$

where the calculable renormalization coefficients $C_i(Q, M_{in}) \rightarrow 0$ as $Q \rightarrow M_{in}$, and, for $M_{in} \geq 10^{11}$ GeV as explored here, $C_i(Q, M_{in}) \rightarrow C_i(Q, M_{GUT})$ monotonically as $M_{in} \rightarrow M_{GUT}$. The coefficients $C_i(Q, M_{in})$ are positive for all the squarks and sleptons, but negative for the Higgs multiplet H_2 that is coupled to the top quark, and also for the other Higgs multiplet H_1 at large $\tan\beta$ when it has large couplings to the bottom quark and τ lepton. These negative corrections make possible dynamical electroweak symmetry breaking, if they drive the full quantity (2) for the corresponding Higgs multiplet negative at low energies. In our treatment

³We note, in passing, that we also assume universality at the same input scale for the soft trilinear supersymmetry-breaking parameters A , though this is not of great relevance for our discussion.

of the sub-GUT CMSSM, we include these effects consistently in the electroweak vacuum conditions.

We see in Figs. 1 and 2 several features related to these renormalization effects. For example, as M_{in} decreases, we see that the requirement that the LSP not be charged (shown as a brick-red shaded region), which imposes the bound $m_{\tilde{\tau}_1} > m_\chi$ (where $\tilde{\tau}_1$ is the lighter stau slepton), encroaches on the allowed region of the $(m_{1/2}, m_0)$ plane from the bottom-right corner. This can be understood from the RGE evolution. As M_{in} decreases, the ratio of the lightest neutralino mass to $m_{1/2}$ increases. Simultaneously, the coefficient $C_{\tilde{\tau}_1}$ decreases as M_{in} decreases. Both effects go in the same direction of requiring a higher value of m_0 for a given value of $m_{1/2}$ in order to enforce $m_{\tilde{\tau}_1} > m_\chi$. We also see a (purple shaded) bound that encroaches on the allowed region of the $(m_{1/2}, m_0)$ plane from the top-left corner, which is due to the change in the electroweak vacuum conditions. The LEP chargino mass constraint lies just within this boundary, and further within the allowed region is a strip where Ω_χ falls within the WMAP range⁴. This shift in this bound can also be traced directly to the diminished RGE evolution, and can be understood qualitatively from the tree-level solution for μ :

$$\mu^2 = \frac{(m_1^2 - m_2^2 \tan^2 \beta)}{\tan^2 \beta - 1} - \frac{M_Z^2}{2} \quad (3)$$

where m_1 and m_2 are the soft Higgs masses associated with H_1 and H_2 and the latter is coupled to the top sector⁵. For low and moderate values of $\tan \beta$, $m_1^2 > 0$ whilst $m_2^2 < 0$ at the weak scale. As M_{in} decreases, the running of m_1 and m_2 is suppressed and, as a result, the absolute values of both remain closer to m_0 . Thus the value of μ at the weak scale is decreased for any fixed values of $m_{1/2}$ and m_0 , and the line where μ^2 changes sign is found at a lower value of m_0 for any fixed value of $m_{1/2}$. The purple shaded regions in Figs. 1 and 2 correspond to regions for which $\mu^2 < 0$, which are therefore unphysical.

Finally, we also see that the lower bound on $m_{1/2}$ due to the LEP Higgs constraint becomes more stringent as M_{in} decreases. This is because $m_h < m_Z$ at the tree level, with a renormalization that is dominated by a logarithmic dependence on $m_{\tilde{t}}$. In turn, we see from (2) that $m_{\tilde{t}}$ increases with $m_{1/2}$, at a rate that is suppressed as M_{in} is decreased. Thus, one requires a progressively higher value of $m_{1/2}$ in order to push the lightest CMSSM Higgs mass above the LEP lower limit $m_h > 114$ GeV.

⁴We return later to its detailed morphology and evolution with M_{in} .

⁵Note that our results are based on full two-loop RGEs and not the simple explanatory approximations given in eqs. 1 - 3.

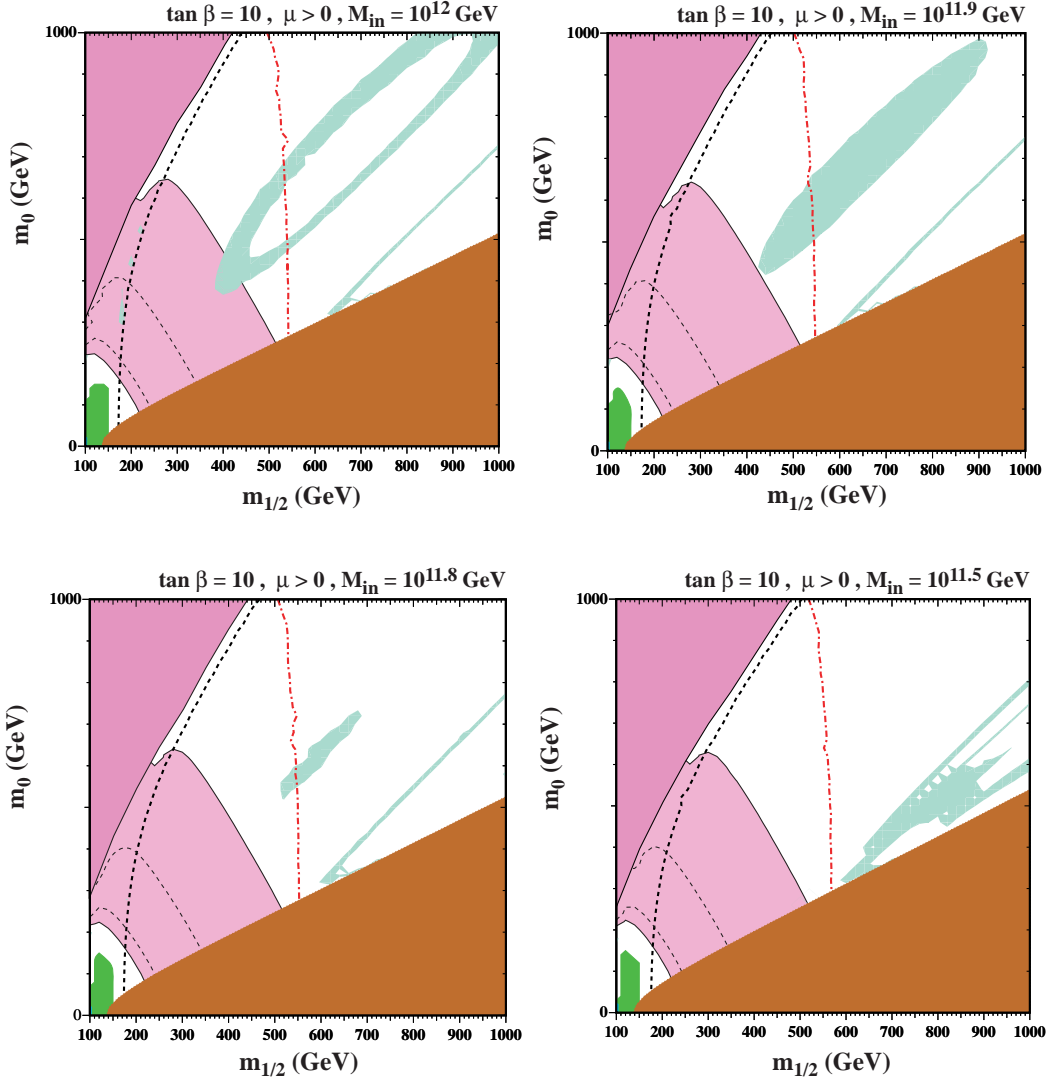


Figure 2: *Examples of $(m_{1/2}, m_0)$ planes with $\tan\beta = 10$ and $A_0 = 0$ but with different values of M_{in} (a) $M_{in} = 10^{12}$ GeV, (b) $M_{in} = 10^{11.9}$ GeV, (c) $M_{in} = 10^{11.8}$ GeV and (d) $M_{in} = 10^{11.5}$ GeV. In each panel, we show the regions excluded by the LEP lower limits on MSSM particles, those ruled out by $b \rightarrow s\gamma$ decay [24, 25] (medium green shading), and those excluded because the LSP would be charged (dark red shading). The region favoured by the WMAP range $\Omega_{CDM}h^2 = 0.1045^{+0.0072}_{-0.0095}$ has light turquoise shading. The region suggested by $g_\mu - 2$ is medium (pink) shaded.*

4 Evolution of the dark matter constraint

We now discuss separately the evolving impact of the WMAP relic-density constraint as M_{in} is decreased for fixed $\tan\beta = 10$ and $\mu > 0$. We see in the usual GUT CMSSM scenario in Fig. 1 the familiar feature of the $\chi - \tilde{\tau}_1$ coannihilation strip at low m_0 , which extends from $m_{1/2} \sim 400$ GeV (where it is cut off by the m_h constraint) up to $m_{1/2} \sim 900$ GeV, where it drops down into the forbidden $\tilde{\tau}_1$ LSP region⁶. There is no funnel region for this value of $\tan\beta$, and the focus-point region is unseen at larger values of m_0 . At low $m_{1/2} \sim 150$ GeV, there is a strip where rapid annihilation via the h pole would bring the χ density into the WMAP range which is, however, forbidden by the LEP chargino constraint and *a fortiori* the LEP Higgs constraint.

The picture starts changing already for $M_{in} = 10^{14}$ GeV, as seen in Fig. 1(b). The electroweak vacuum condition is visible at $(m_{1/2}, m_0) \sim (200, 1000)$ GeV, with the chargino constraint close by, and a WMAP strip tracking its boundary with $m_0 \sim 200$ GeV lower. This WMAP strip does not join directly with the coannihilation strip, but is instead deflected via a section of the rapid h annihilation strip at $m_{1/2} \sim 150$ GeV. This behaviour is linked to the $\chi\chi \rightarrow WW$ channel, which has a significant threshold in $m_{1/2}$, but whose importance varies with $m_{1/2}$ and m_0 . The rate of variation of the relic density in this region is reflected in the thickness of the WMAP-allowed region. For example, if we follow the relic density at fixed $m_0 = 600$ GeV, we find that at small $m_{1/2}$, the relic density is low due to the rapid annihilation through the light Higgs. As $m_{1/2}$ is increased, the density increases and at $m_{1/2} \simeq 170 - 190$ GeV, the density is too high. However at slightly higher $m_{1/2}$, the WW channel opens up, and because μ is lower relative to its value in the GUT-CMSSM, the relic density drops and becomes small at $m_{1/2} \lesssim 200$ GeV. As one moves away from the forbidden triangle in the upper left, μ begins to increase, and the relic density again begins to increase so that the relic density is too large when $m_{1/2} \gtrsim 240$ GeV. Thus, along this horizontal line, we have passed through three regions for which we match the WMAP relic density. The coannihilation strip is rather similar to that in the GUT CMSSM case shown in Fig. 1(a).

There is a more dramatic change for $M_{in} = 10^{13}$ GeV, as seen in Fig. 1(c). Not only has the electroweak vacuum constraint encroached further on the $(m_{1/2}, m_0)$ plane, but also the focus-point WMAP strip has receded further away from it, appearing at $m_0 \sim 300$ GeV lower. Moreover, this focus-point strip now connects smoothly at $m_{1/2} \sim 250$ GeV with the $\chi - \tilde{\tau}_1$ coannihilation strip at low m_0 . The coannihilation strip itself exhibits some broadening

⁶If the gravitino were light, the $\tilde{\tau}_1$ would become the NLSP in this region, and there would be an allowed region with gravitino dark matter, but we do not explore this possibility here.

and embryonic bifurcation at $m_{1/2} \sim 1000$ GeV, due to the approaching funnel.

The emerging picture is much clearer in Fig. 1(d), where $M_{in} = 10^{12.5}$ GeV. The focus-point part of the WMAP strip has now separated further from the electroweak vacuum boundary, but also the linked ‘coannihilation’ portion of the WMAP strip has separated from the $\tilde{\tau}_1$ LSP boundary, by an amount that increases with $m_{1/2}$. In fact, we now recognize the region at large $m_{1/2}$ as the opening of a characteristic rapid A, H annihilation funnel, of the type seen in the GUT CMSSM only when $\tan\beta \sim 50$ for $\mu > 0$ as studied here. On the further side of the funnel, at $m_{1/2} \sim 900$ GeV, we now see more clearly the bifurcation of the second funnel wall from the continuing coannihilation strip.

The changes described above accelerate as M_{in} decreases further, as seen in Fig. 2. For $M_{in} = 10^{12}$ GeV, as seen in Fig. 2(a), the former focus-point, lower coannihilation and funnel regions merge into a WMAP ellipse that encloses just a small region where the χ relic density is too large. The further wall of the funnel and the continuation of the coannihilation strip form a well-developed ‘vee’ shape that extends to much larger values of $m_{1/2}$ than those shown here.

Even more strikingly, when M_{in} is reduced slightly to $10^{11.9}$ GeV, as shown in Fig. 2(b), the ellipse is now filled up. This is the culmination of a trend, noticeable already in Fig. 1, for the WMAP regions to broaden as well as merge as M_{in} decreases. The possibility that the LSP relic density falls within the WMAP range therefore appears more ‘natural’. Moreover, we see in Fig. 2(a), (b) that it is increasingly ‘unlikely’ that the relic density will exceed the WMAP range, whereas this appeared much more ‘likely’ in the GUT CMSSM case shown in Fig. 1(a). Whether one worries about the ‘naturalness’ of supersymmetric dark matter or not, it is nevertheless interesting that there is less cause for worry when $M_{in} \sim 10^{12}$ GeV.

The situation changes again with just a small change to $M_{in} = 10^{11.8}$ GeV, as seen in Fig. 1. The ellipse has now almost evaporated, with the relic density falling below the range favoured by WMAP over most of the visible part of the $(m_{1/2}, m_0)$ plane⁷. The only region with an excessive amount of cold dark matter is inside the ‘vee’ at large $m_{1/2}$. Note also, that the region favoured by the relic density no longer overlaps with the region preferred by the $g_\mu - 2$ anomaly.

Finally, when $M_{in} = 10^{11.5}$ GeV, as shown in Fig. 1(d), the ellipse favoured by WMAP has disappeared completely. We also notice that the large- $m_{1/2}$ ‘vee’ starts to fill in, with a new generic region of acceptable relic density now appearing. This is due, in particular, to the opening up of new annihilation channels such $(H, A) + Z, H^\pm + W^\mp$ that are sufficient

⁷These regions would of course still be acceptable for cosmology, if there were another important source of cold dark matter.

to bring the relic density down into the WMAP range. At lower values of $M_{in} \rightarrow 10^{10}$ GeV (not shown), the electroweak vacuum boundary continues to press downwards and the relic density is always below the favoured WMAP range for $m_\chi < m_A/2$. The relic density lies within the WMAP range only along narrow strips close to the top and bottom of the ‘vee’ where $m_\chi \geq m_A/2, m_{\tilde{\tau}_1}$. To better understand this behaviour, let us look at the density at fixed $m_{1/2} = 900$ GeV. At large m_0 , the annihilation cross section is large dominated by the broad s-channel pole through the heavy Higgses, H and A . As m_0 is lowered, $2m_\chi$ becomes larger than m_A , and at $m_0 \approx 700$, the WMAP density is attained. As one moves to lower m_0 , away from the pole, the relic density increases, but the heavy Higgs masses decrease opening up the $H^\pm + W^\mp$ channel when $m_0 \approx 630$ GeV and the $(H, A) + Z$ at slightly lower m_0 . In this region of the parameter space, the s-wave annihilation cross section is dominant and decreases as m_0 is lowered, so there is a modest increase in the density and the WMAP value is obtained again when $m_0 \lesssim 600$ GeV. At still lower m_0 , yet another channel opens up. At $m_0 \lesssim 560$ GeV, the h, A channel is open and the density once again drops below the WMAP value. As we continue to move off of the Higgs funnel, the h, A contribution slowly decreases and the density rises and surpasses the WMAP value. At this value of $m_{1/2}$, we are past the endpoint of $\chi - \tilde{\tau}$ coannihilation and the density is too large as we enter the $\tilde{\tau}$ LSP region.

If we continue to lower the supersymmetry breaking input scale, M_{in} , we find that the region seen in Fig. 1(d) begins to evaporate. At $M_{in} = 10^{11.2}$ GeV, it is gone, but the $\chi - \tilde{\tau}$ coannihilation region has returned for $M_{1/2} \gtrsim 600$ GeV. The lower end of the coannihilation region continues to move to higher $M_{1/2}$ as M_{in} is decreased, so that when $M_{in} < 10^{10}$ GeV, the lower end of the coannihilation region is at $M_{1/2} \approx 900$ GeV.

5 Evolution of sparticle masses

We now discuss the extent to which the results presented in the previous Section can be understood in terms of the evolution of sparticle masses with M_{in} , and the corresponding implications for and of sparticle measurements at colliders such as the LHC.

We display in Fig. 3 two examples of the evolution of sparticle mass parameters with M_{in} in the focus-point region. Panel (a) is for $(m_{1/2}, m_0) = (200, 1000)$ GeV, and panel (b) for $(m_{1/2}, m_0) = (500, 1000)$ GeV. In each case, we show the evolution of the un-mixed electroweak gaugino mass M_1 (blue dotted lines), the Higgs soft mass represented by $sgn(m_2^2)(\sqrt{|m_2^2|})$ (turquoise dot-dashed lines), the absolute value of μ (red dashed lines) and the LSP mass m_χ (solid black line). We see that, as M_{in} decreases from the GUT

value of 2×10^{16} GeV, both $|\sqrt{m_2^2}|$ and particularly $|\mu|$ plummet precipitously, whereas the gaugino masses $M_{1,2}$ evolve more slowly. In the GUT CMSSM, m_χ is essentially equal to M_1 , but this changes as M_{in} decreases, and m_χ is given by $|\mu|$ when this is small. In both the examples shown, the first disaster to occur as M_{in} decreases is that $|\mu|$ vanishes, which marks the boundary of the region of the $(m_{1/2}, m_0)$ plane allowed by the electroweak vacuum conditions. The disallowed regions are shaded (purple): this boundary reaches the point $(m_{1/2}, m_0) = (200, 1000)$ GeV shown in panel (a) when $M_{in} \sim 10^{14.5}$ GeV, whereas Armageddon is postponed until $M_{in} \sim 10^{11.4}$ GeV for the point $(m_{1/2}, m_0) = (500, 1000)$ GeV shown in panel (b). In both the cases studied, $\sqrt{|m_2^2|}$ does not vanish until well inside the region disallowed by the electroweak vacuum conditions. We have seen the consequences of this behavior in Figs. 1 and 2 as the encroachment of the region where the electroweak symmetry breaking conditions are not obeyed.

In panel (a), the relic neutralino density exceeds the WMAP upper limit in the GUT CMSSM, and the relic density falls as M_{in} decreases. There is a narrow range of $M_{in} \sim 10^{15}$ GeV where the density falls within the favoured WMAP range, and it then falls to zero as $|\mu|$ and hence m_χ vanishes. In panel (b), there is a similar sequence of events, with the WMAP range attained at a lower value of $M_{in} \sim 10^{13.2}$ GeV.

Panels (c) and (d) of Fig. 3 provide analogous displays of the evolution of mass parameters with M_{in} in the funnel region, for $(m_{1/2}, m_0) = (1000, 400)$ GeV and $(m_{1/2}, m_0) = (1000, 800)$ GeV, respectively. Here, in addition to M_1 , μ , $|\sqrt{m_2^2}|$ and m_χ , we also plot $m_{\tilde{\tau}_1}$ and $m_{A/2}$. The evolution of $m_{\tilde{\tau}_1}$ is undramatic. As in panels (a) and (b), the physical region is bounded by the vanishing of μ and hence m_χ , which occurs at $M_{in} \sim 10^{6.5}$ GeV and $M_{in} \sim 10^{8.3}$ GeV in cases (c) and (d), respectively. As in the cases (a) and (b), the LSP mass tracks M_1 at large M_{in} and then μ at smaller M_{in} after the values of μ and M_1 cross.

Among the more interesting aspects of panels (c) and (d) are the comparisons between m_χ and $m_{\tilde{\tau}_1}$, on the one hand, and between m_χ and $m_{A/2}$, on the other hand. In panel (c), we see that m_χ rises above $m_{\tilde{\tau}_1}$ (which is unacceptable) when M_{in} falls to $\sim 10^{14}$ GeV, a feature visible also in panel (b) of Fig. 1, where we notice that the point $(m_{1/2}, m_0) = (1000, 400)$ GeV sits on the boundary of the stau LSP region for this value of M_{in} . We also note that m_χ falls (with μ) below $m_{\tilde{\tau}_1}$ when $M_{in} < 10^9$ GeV, an effect not visible in our previous scans of the $(m_{1/2}, m_0)$ planes in Figs. 1 and 2, where we only considered $M_{in} \geq 10^{11.5}$ GeV. In panel (d), we again see the crossover from $m_\chi \sim M_1$ to $m_\chi \sim \mu$, whereas $m_{\tilde{\tau}_1} > m_\chi$ in this case.

Comparing now m_χ with $m_{A/2}$, we see in panel (c) that in the case $(m_{1/2}, m_0) = (1000, 400)$ GeV they become equal only in the stau LSP region when $M_{in} \sim 10^{13}$ GeV, whereas in the case $(m_{1/2}, m_0) = (1000, 800)$ GeV shown in panel (d) m_χ and $m_{A/2}$ be-

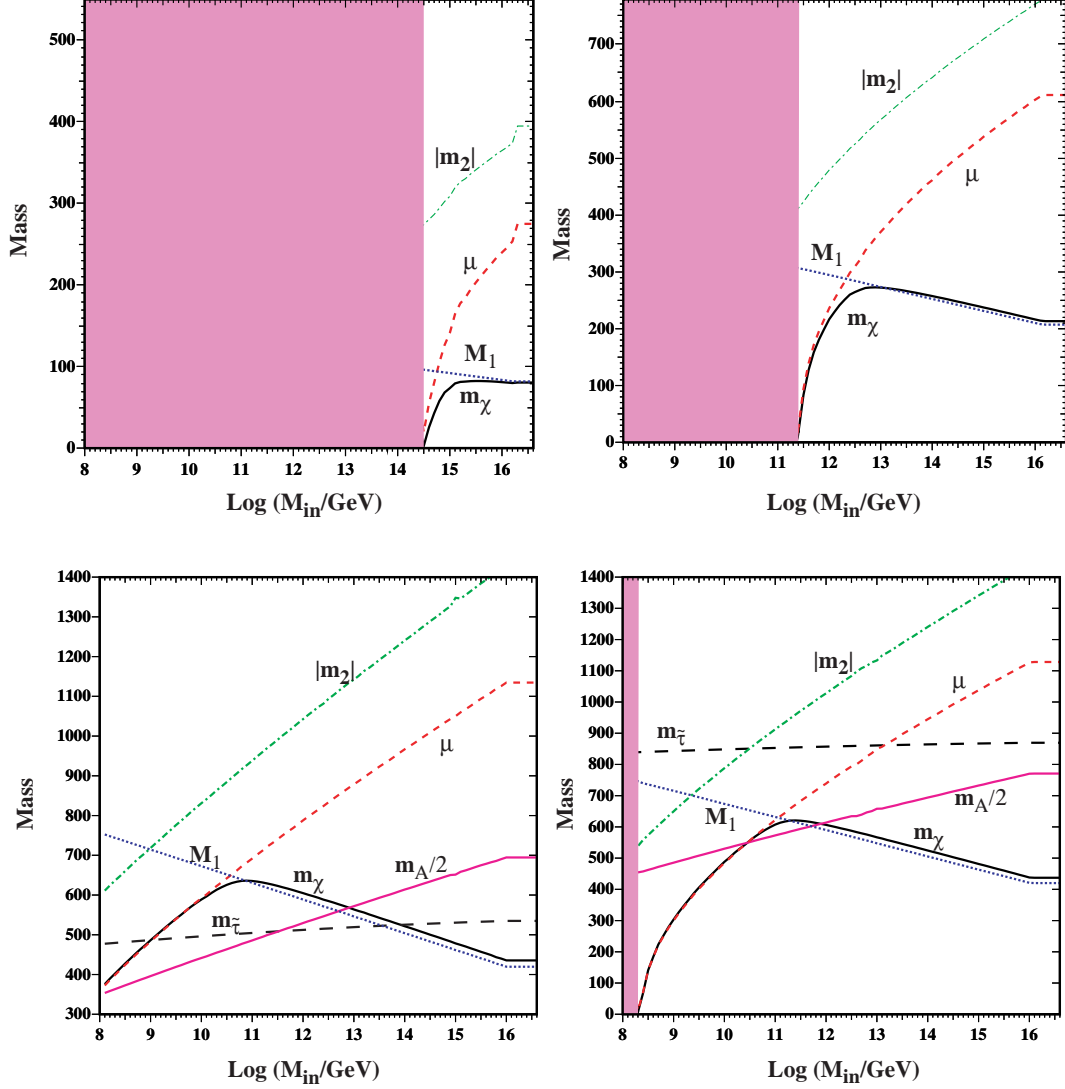


Figure 3: Mass parameters as functions of M_{in} in the focus-point region, for (a) $(m_{1/2}, m_0) = (200, 1000)$ GeV, and (b) $(m_{1/2}, m_0) = (500, 1000)$ GeV, and in the funnel region for (c) $(m_{1/2}, m_0) = (1000, 400)$ GeV, and (d) $(m_{1/2}, m_0) = (1000, 800)$ GeV.

come equal twice, when $M_{in} \sim 10^{12}$ and $10^{10.5}$ GeV, and m_χ and $m_A/2$ are quite similar for intermediate and adjacent values of M_{in} .

Since the relation between m_χ and $m_{\tilde{\tau}_1}$ is very important for coannihilation, and that between m_χ and $m_A/2$ is very important for the rapid-annihilation funnel, these crossover patterns have important effects on the relic χ density, and enable us to understand some features of Figs. 1 and 2. Specifically, for $(m_{1/2}, m_0) = (1000, 400)$ GeV as shown in panel (c) of Fig. 3, the approach towards $m_\chi = m_{\tilde{\tau}_1}$ as $M_{in} \rightarrow 10^{14}$ GeV is responsible for a significant reduction in the dark matter density. The relic density is also reduced for the case $(m_{1/2}, m_0) = (1000, 800)$ GeV shown in panel (d) of Fig. 3 as $M_{in} \rightarrow 10^{12.5}$ GeV, as also seen in Fig. 1. The relic density then remains below the range favoured by WMAP as $M_{in} \rightarrow 10^{11.8}$ GeV, as seen in the first three panels of Fig. 2. On the other hand, the density rises to the favoured WMAP range when $M_{in} = 10^{11.5}$ GeV, and would even exceed the WMAP range for smaller values of M_{in} . This is because m_χ is now greater than $m_A/2$. However, we expect the density to fall again as M_{in} decreases further and m_χ decreases again and crosses $m_A/2$ a second time.

6 Implications for collider searches

It is clear that the prospects for searches for supersymmetry at the LHC and other colliders depend on the value of M_{in} assumed. One may also ask to what extent collider measurements could be used to extract the value of M_{in} , at least within a specific CMSSM framework. These are complicated issues whose full investigation would extend far beyond the scope of this exploratory study. Here we restrict our attention to two specific scans across the $(m_{1/2}, m_0)$ plane for $\tan\beta = 10$ and $\mu > 0$ as functions of M_{in} , shown in Fig. 4. In scan (a), we first fix $m_{1/2} = 700$ GeV and then, for each value of M_{in} , find the value(s) of m_0 that yield a relic density within the range favoured by WMAP. Then, for each of these WMAP-compatible choices of m_0 , we calculate the masses of some interesting sparticles, namely χ , $\tilde{\tau}_1$, χ_2 , \tilde{q}_R and \tilde{g} and finally we plot their dependences on M_{in} . In scan (b), we instead first fix $m_0 = 700$ GeV, then find, for each value of M_{in} , the value(s) of $m_{1/2}$ yielding the WMAP relic density, and finally plot the same set of masses as functions of M_{in} .

In the case of the first scan at fixed $m_{1/2} = 700$ GeV shown in Fig. 4(a), as M_{in} decreases from 2×10^{16} GeV towards 10^{13} GeV, we see that $m_{\tilde{g}}$ and $m_{\tilde{q}_R}$ decrease gradually, whereas m_χ , $m_{\tilde{\tau}_1}$ and m_{χ_2} increase gradually. The behaviours of $m_{\tilde{g}}$ and m_χ are simply due to their reduced mass renormalizations as M_{in} decreases. In the case of $m_{\tilde{\tau}_1}$, at large M_{in} , one must choose m_0 to lie within the WMAP coannihilation strip, so that the relic density remains

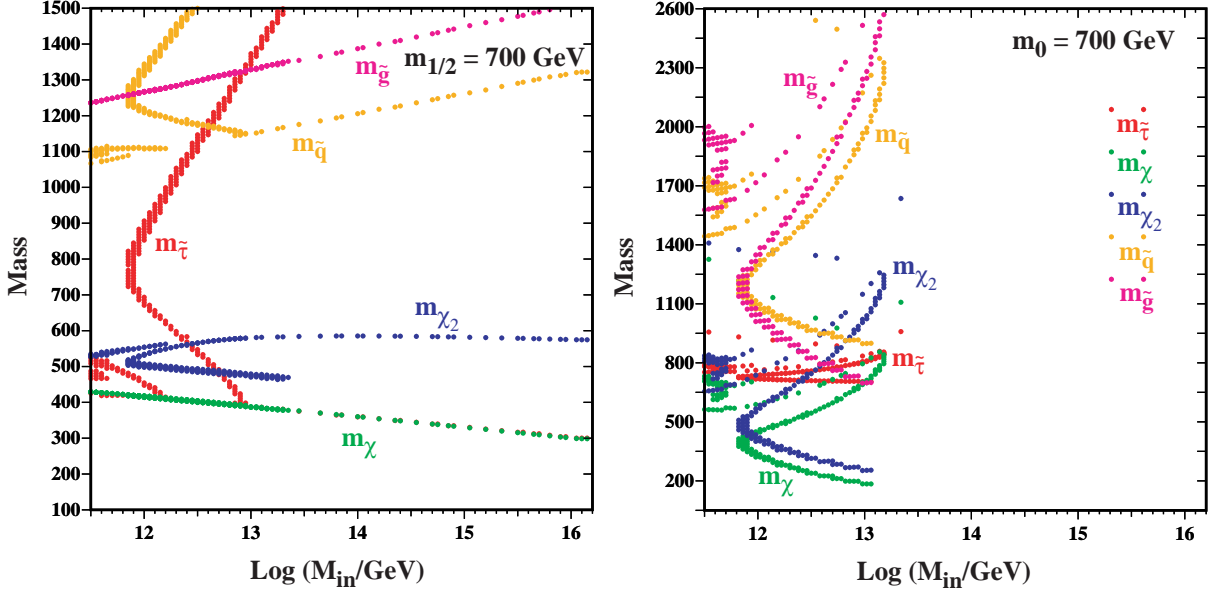


Figure 4: *Sparticle masses for sub-GUT CMSSM models chosen to be compatible with the WMAP relic-density constraint for $\tan\beta = 10$, $A = 0$, $\mu > 0$ and (a) $m_{1/2} = 700$ GeV, (b) $m_0 = 700$ GeV. For each value of M_{in} , we choose (a) m_0 and (b) $m_{1/2}$ so as to respect WMAP, and then plot the corresponding sparticle masses as functions of M_{in} .*

within the allowed range. This requires $m_{\tilde{\tau}_1}$ to be only very slightly larger than m_{χ^0} ⁸, so it also increases as M_{in} decreases. In the case of $m_{\tilde{q}_R}$, there are effects due to both the reduced mass renormalization and the WMAP-induced change in m_0 , the former being dominant. A new phenomenon appears as $M_{in} \rightarrow 10^{13}$ GeV, namely, as seen in Fig. 1(d), the WMAP strip at small m_0 moves away from the coannihilation limit, and $m_{\tilde{\tau}_1}$ increases much more rapidly than m_{χ^0} . Also, a new branch of the WMAP strip appears⁹ at large m_0 , in which $m_{\tilde{\tau}_1}$ decreases as $M_{in} \rightarrow 10^{12}$ GeV: similar behaviour is apparent for $m_{\tilde{q}_R}$. For points in the upper m_0 branch, the χ_2 has a lower mass and is predominantly Higgsino in content, whereas in the lower m_0 branch the χ_2 is mostly wino. When $M_{in} \sim 10^{12}$ GeV as shown in Fig. 2, the two branches of the WMAP strip merge, as do the two possible values of $m_{\tilde{\tau}_1}$, $m_{\tilde{q}_R}$ and m_{χ_2} . However, appearing already at M_{in} slightly larger than 10^{12} GeV, we see new, somewhat lower ranges of allowed values of $m_{\tilde{\tau}_1}$ and $m_{\tilde{q}_R}$ (and higher values of m_{χ_2}), which correspond to the wedge of allowed m_0 values inside the ‘vee’ visible in Fig. 1(d) for $m_{1/2}$ beyond the rapid-annihilation funnel. It is apparent that the spectra allowed by

⁸For this reason, the (red) $\tilde{\tau}_1$ points are scarcely visible along the (green) χ line.

⁹This branch, associated with the focus point, exists at larger M_{in} as well, but it does not appear in our scan, because it only extends to $m_0 = 1500$ GeV.

WMAP are very sensitive to the assumed value of M_{in} . For example, a determination of the ratio $m_\chi/m_{\tilde{g}}$ with an accuracy of 4 % (which may be possible at the LHC) would by itself fix M_{in} to within an order of magnitude, in the restricted set of models considered here.

In the case of the second scan at $m_0 = 700$ GeV, we see in Fig. 1 that due to the Higgs mass bound (we use here the value of 112 GeV calculated using `FeynHiggs`, so as to account for theoretical uncertainties), a suitable WMAP strip appears only when $M_{in} \lesssim 10^{13}$ GeV, and this is reflected in the disappearance of the sparticle mass lines just above $M_{in} = 10^{13}$ GeV in Fig. 4(b). As M_{in} decreases, two of the branches for each sparticle mass merge. However, there are two other branches, one appearing near $M_{in} \sim 10^{13}$ GeV and the other closer to $M_{in} \sim 10^{12}$ GeV. These are due to the appearance of the WMAP-allowed ‘vee’ seen close to the $m_\chi = m_{\tilde{\tau}_1}$ line in Fig. 1(d) *et seq.*. In this case, we see that the WMAP-allowed values of the sparticle masses vary rapidly for $M_{in} \in (10^{12}, 10^{13})$ GeV. This another example how LHC measurements of sparticle masses would help fix the magnitude of M_{in} in this restricted set of models.

7 Discussion

We have presented a first exploration of the dependence of the $(m_{1/2}, m_0)$ plane for $\tan \beta = 10, A = 0, \mu > 0$ on the scale M_{in} at which the input soft supersymmetry-breaking CMSSM mass parameters $m_{1/2}$ and m_0 are assumed to be universal. We have displayed and explained how the phenomenological, experimental and cosmological constraints vary with M_{in} . In particular, we have shown that the morphology of the region favoured by the WMAP range of the relic density changes with M_{in} . Specifically, the focus point region at large m_0 the coannihilation strip and the rapid-annihilation funnel at large $m_{1/2}$ approach each other and merge as M_{in} decreases to $\sim 10^{12}$ GeV. Consequently, the values of the sparticle masses that would be compatible with WMAP depend on M_{in} , and measurements at the LHC may be able to offer some hints about the value of M_{in} within such sub-GUT CMSSM scenarios.

It is desirable to extend this discussion to other values of the CMSSM parameters $\tan \beta$ and A . It would also be interesting to extend this analysis to less constrained versions of the MSSM, such as models with non-universal Higgs masses, and also more constrained versions of the MSSM motivated by minimal supergravity. It would also be valuable to extend the brief discussion given here of the corresponding spectra and the prospects for the LHC and ILC to ‘measure’ indirectly the value of M_{in} . We plan to return to these issues in a future paper.

Acknowledgments

The work of K.A.O. and P.S. was supported in part by DOE grant DE-FG02-94ER-40823.

References

- [1] E. Witten, Nucl. Phys. B **188** (1981) 513; N. Sakai, Z. Phys. C **11** (1981) 153; S. Dimopoulos and H. Georgi, Nucl. Phys. B **193** (1981) 150; R. K. Kaul and P. Majumdar, Nucl. Phys. B **199** (1982) 36.
- [2] J. R. Ellis, S. Kelley and D. V. Nanopoulos, Phys. Lett. B **260** (1991) 131; U. Amaldi, W. de Boer and H. Furstenuau, Phys. Lett. B **260** (1991) 447; P. Langacker and M. x. Luo, Phys. Rev. D **44** (1991) 817; C. Giunti, C. W. Kim and U. W. Lee, Mod. Phys. Lett. A **6** (1991) 1745.
- [3] J. Ellis, J.S. Hagelin, D.V. Nanopoulos, K.A. Olive and M. Srednicki, Nucl. Phys. B **238** (1984) 453; see also H. Goldberg, Phys. Rev. Lett. **50** (1983) 1419.
- [4] J. R. Ellis, G. Ridolfi and F. Zwirner, Phys. Lett. B **257** (1991) 83; Phys. Lett. B **262** (1991) 477; A. Yamada, Phys. Lett. B **263**, 233 (1991); M. Drees and M. M. Nojiri, Phys. Rev. D **45** (1992) 2482; P. H. Chankowski, S. Pokorski and J. Rosiek, Phys. Lett. B **274** (1992) 191; Phys. Lett. B **286** (1992) 307; A. Dabelstein, Z. Phys. C **67** (1995) 495 [arXiv:hep-ph/9409375]; M. Carena, J. R. Ellis, A. Pilaftsis and C. E. M. Wagner, Nucl. Phys. B **586** (2000) 92 [arXiv:hep-ph/0003180]; A. Katsikatsou, A. B. Lahanas, D. V. Nanopoulos and V. C. Spanos, Phys. Lett. B **501** (2001) 69 [arXiv:hep-ph/0011370].
- [5] E. Cremmer, B. Julia, J. Scherk, S. Ferrara, L. Girardello and P. Van Nieuwenhuizen, Phys. Lett. **79B** (1978) 231; and Nucl. Phys. **B147** (1979) 105; E. Cremmer, S. Ferrara, L. Girardello and A. Van Proeyen, Phys. Lett. **116B** (1982) 231; and Nucl. Phys. **B212** (1983) 413; R. Arnowitt, A.H. Chamseddine and P. Nath, Phys. Rev. Lett. **49** (1982) 970; **50** (1983) 232 and Phys. Lett. **121B** (1983) 33; J. Bagger and E. Witten, Phys. Lett. **115B** (1982) 202 and **118B** (1982) 103; J. Bagger, Nucl. Phys. **B211** (1983) 302.
- [6] For reviews, see: H. P. Nilles, Phys. Rep. **110** (1984) 1; A. Brignole, L. E. Ibanez and C. Munoz, arXiv:hep-ph/9707209, published in *Perspectives on supersymmetry*, ed. G. L. Kane, pp. 125-148.

- [7] J. Polonyi, Budapest preprint KFKI-1977-93 (1977).
- [8] R. Barbieri, S. Ferrara and C.A. Savoy, *Phys. Lett.* **119B** (1982) 343.
- [9] For a review see e.g. H. E. Haber and G. L. Kane, *Phys. Rept.* **117** (1985) 75.
- [10] M. Drees and M. M. Nojiri, *Phys. Rev. D* **47** (1993) 376 [arXiv:hep-ph/9207234]; H. Baer and M. Brhlik, *Phys. Rev. D* **53** (1996) 597 [arXiv:hep-ph/9508321] J. R. Ellis, T. Falk, K. A. Olive and M. Schmitt, *Phys. Lett. B* **388** (1996) 97 [arXiv:hep-ph/9607292]; *Phys. Lett. B* **413** (1997) 355 [arXiv:hep-ph/9705444]; J. R. Ellis, T. Falk, G. Ganis, K. A. Olive and M. Schmitt, *Phys. Rev. D* **58** (1998) 095002 [arXiv:hep-ph/9801445]; J. R. Ellis, T. Falk, G. Ganis and K. A. Olive, *Phys. Rev. D* **62** (2000) 075010 [arXiv:hep-ph/0004169]; V. D. Barger and C. Kao, *Phys. Rev. D* **57** (1998) 3131 [arXiv:hep-ph/9704403].
- [11] J. R. Ellis, T. Falk, G. Ganis, K. A. Olive and M. Srednicki, *Phys. Lett. B* **510** (2001) 236 [arXiv:hep-ph/0102098].
- [12] V. D. Barger and C. Kao, *Phys. Lett. B* **518** (2001) 117 [arXiv:hep-ph/0106189]; L. Roszkowski, R. Ruiz de Austri and T. Nihei, *JHEP* **0108** (2001) 024 [arXiv:hep-ph/0106334]; A. B. Lahanas and V. C. Spanos, *Eur. Phys. J. C* **23** (2002) 185 [arXiv:hep-ph/0106345]; A. Djouadi, M. Drees and J. L. Kneur, *JHEP* **0108** (2001) 055 [arXiv:hep-ph/0107316]; U. Chattopadhyay, A. Corsetti and P. Nath, *Phys. Rev. D* **66** (2002) 035003 [arXiv:hep-ph/0201001]; J. R. Ellis, K. A. Olive and Y. Santoso, *New Jour. Phys.* **4** (2002) 32 [arXiv:hep-ph/0202110]; H. Baer, C. Balazs, A. Belyaev, J. K. Mizukoshi, X. Tata and Y. Wang, *JHEP* **0207** (2002) 050 [arXiv:hep-ph/0205325]; R. Arnowitt and B. Dutta, arXiv:hep-ph/0211417.
- [13] J. R. Ellis, K. A. Olive, Y. Santoso and V. C. Spanos, *Phys. Lett. B* **565** (2003) 176 [arXiv:hep-ph/0303043]; H. Baer and C. Balazs, arXiv:hep-ph/0303114; A. B. Lahanas and D. V. Nanopoulos, arXiv:hep-ph/0303130; U. Chattopadhyay, A. Corsetti and P. Nath, arXiv:hep-ph/0303201; C. Munoz, hep-ph/0309346.
- [14] J. R. Ellis, K. A. Olive, Y. Santoso and V. C. Spanos, *Phys. Rev. D* **69** (2004) 095004 [arXiv:hep-ph/0310356]; J. Ellis, S. Heinemeyer, K. Olive and G. Weiglein, *JHEP* **0502** 013, hep-ph/0411216; B. Allanach and C. Lester, *Phys. Rev. D* **73** (2006) 015013, hep-ph/0507283; B. Allanach, hep-ph/0601089; R. de Austri, R. Trotta and L. Roszkowski, hep-ph/0602028; J. Ellis, S. Heinemeyer, K. A. Olive and G. Weiglein, arXiv:hep-ph/0602220.

- [15] A. Corsetti and P. Nath, Phys. Rev. D **64** (2001) 125010 [arXiv:hep-ph/0003186]; R. Arnowitt, B. Dutta and Y. Santoso, Nucl. Phys. B **606** (2001) 59 [arXiv:hep-ph/0102181]; D. G. Cerdeno, E. Gabrielli, S. Khalil, C. Munoz, E. Torrente-Lujan and E. Torrente-Lujan, Nucl. Phys. B **603** (2001) 231 [arXiv:hep-ph/0102270].
- [16] D. N. Spergel *et al.*, [arXiv:astro-ph/0603449].
- [17] J. R. Ellis, T. Falk and K. A. Olive, Phys. Lett. B **444** (1998) 367 [arXiv:hep-ph/9810360]; J. R. Ellis, T. Falk, K. A. Olive and M. Srednicki, Astropart. Phys. **13** (2000) 181 [Erratum-ibid. **15** (2001) 413] [arXiv:hep-ph/9905481]; R. Arnowitt, B. Dutta and Y. Santoso, Nucl. Phys. B **606** (2001) 59 [arXiv:hep-ph/0102181]; M. E. Gómez, G. Lazarides and C. Pallis, Phys. Rev. D **D61** (2000) 123512 [arXiv:hep-ph/9907261]; Phys. Lett. **B487** (2000) 313 [arXiv:hep-ph/0004028]; Nucl. Phys. B **B638** (2002) 165 [arXiv:hep-ph/0203131]; T. Nihei, L. Roszkowski and R. Ruiz de Austri, JHEP **0207** (2002) 024 [arXiv:hep-ph/0206266].
- [18] J. L. Feng, K. T. Matchev and T. Moroi, Phys. Rev. Lett. **84** (2000) 2322; J. L. Feng, K. T. Matchev and T. Moroi, Phys. Rev. **D61** (2000) 075005; J. L. Feng, K. T. Matchev and F. Wilczek, Phys. Lett. **B482** (2000) 388.
- [19] H. Baer and M. Brhlik, Phys. Rev. D **53** (1996) 597 [arXiv:hep-ph/9508321]; H. Baer, M. Brhlik, M. A. Diaz, J. Ferrandis, P. Mercadante, P. Quintana and X. Tata, Phys. Rev. D **63** (2001) 015007 [arXiv:hep-ph/0005027]; A. B. Lahanas and V. C. Spanos, Eur. Phys. J. C **23** (2002) 185 [arXiv:hep-ph/0106345].
- [20] Tevatron Electroweak Working Group, *Combination of CDF and D0 results on the mass of the top quark*, arXiv:hep-ex/0603039.
- [21] Joint LEP 2 Supersymmetry Working Group, *Combined LEP Chargino Results up to 208 GeV*,
http://lepsusy.web.cern.ch/lepsusy/www/inos_moriond01/charginos_pub.html.
- [22] LEP Higgs Working Group for Higgs boson searches, OPAL Collaboration, ALEPH Collaboration, DELPHI Collaboration and L3 Collaboration, Phys. Lett. B **565** (2003) 61 [arXiv:hep-ex/0306033]. *Search for neutral Higgs bosons at LEP*, paper submitted to ICHEP04, Beijing, LHWG-NOTE-2004-01, ALEPH-2004-008, DELPHI-2004-042, L3-NOTE-2820, OPAL-TN-744,
http://lephiggs.web.cern.ch/LEPHIGGS/papers/August2004_MSSM/index.html.

- [23] S. Heinemeyer, W. Hollik and G. Weiglein, *Comput. Phys. Commun.* **124** (2000) 76 [arXiv:hep-ph/9812320]; S. Heinemeyer, W. Hollik and G. Weiglein, *Eur. Phys. J. C* **9** (1999) 343 [arXiv:hep-ph/9812472].
- [24] S. Chen *et al.* [CLEO Collaboration], *Phys. Rev. Lett.* **87** (2001) 251807 [arXiv:hep-ex/0108032]; P. Koppenburg *et al.* [Belle Collaboration], *Phys. Rev. Lett.* **93** (2004) 061803 [arXiv:hep-ex/0403004]. B. Aubert *et al.* [BaBar Collaboration], arXiv:hep-ex/0207076.
- [25] M. Ciuchini, G. Degrossi, P. Gambino and G. F. Giudice, *Nucl. Phys. B* **527** (1998) 21 [arXiv:hep-ph/9710335]; *Nucl. Phys. B* **534** (1998) 3 [arXiv:hep-ph/9806308]; C. Degrossi, P. Gambino and G. F. Giudice, *JHEP* **0012** (2000) 009 [arXiv:hep-ph/0009337]; M. Carena, D. Garcia, U. Nierste and C. E. Wagner, *Phys. Lett. B* **499** (2001) 141 [arXiv:hep-ph/0010003]; P. Gambino and M. Misiak, *Nucl. Phys. B* **611** (2001) 338; D. A. Demir and K. A. Olive, *Phys. Rev. D* **65** (2002) 034007 [arXiv:hep-ph/0107329]; F. Borzumati, C. Greub and Y. Yamada, *Phys. Rev. D* **69** (2004) 055005 [arXiv:hep-ph/0311151]; T. Hurth, *Rev. Mod. Phys.* **75** (2003) 1159 [arXiv:hep-ph/0212304].
- [26] G. W. Bennett *et al.* [Muon g-2 Collaboration], *Phys. Rev. Lett.* **92** (2004) 161802 [arXiv:hep-ex/0401008]; M. Davier, S. Eidelman, A. Hocker and Z. Zhang, *Eur. Phys. J. C* **31** (2003) 503 [arXiv:hep-ph/0308213]; K. Hagiwara, A. D. Martin, D. Nomura and T. Teubner, arXiv:hep-ph/0312250; J. F. de Trocóniz and F. J. Ynduráin, arXiv:hep-ph/0402285; K. Melnikov and A. Vainshtein, arXiv:hep-ph/0312226; M. Passera, arXiv:hep-ph/0411168.